INL/RPT-22-70037
Revision 0

Multicomponent Nanoparticle Synthesis for Advanced Manufactured Melt Wire Development

October 2022

Kiyo T. Fujimoto and Kennalee Orme
Idaho National Laboratory

Nicholas Der Garabedian
Idaho National Laboratory and Villanova University

Idaho National Laboratory

INL is a U.S. Department of Energy National Laboratory operated by Battelle Energy Alliance, LLC

INL/RPT-22-70037
Revision 0

Multicomponent Nanoparticle Synthesis for Advanced Manufactured Melt Wire Development

Kiyo T. Fujimoto and Kennalee Orme
Idaho National Laboratory
Nicholas Der Garabedian
Idaho National Laboratory and Villanova University

October 2022

Idaho National Laboratory
Idaho Falls, Idaho 83415

http://www.inl.gov

Prepared for the
U.S. Department of Energy
Office of Nuclear Energy
Under DOE Idaho Operations Office
Contract DE-AC07-05ID14517

Page intentionally left blank

ABSTRACT

Additive manufacturing (AM)-based direct-write technologies have emerged as a predominant enabler for the fabrication of advanced passive sensors in-pile applications. This work continues previous efforts with the modification and optimization of synthesis methods for multicomponent nanoparticle systems used to support the development, fabrication, and testing of AM sensors for peak temperature detection. For this report, bismuth, bismuth/platinum, tin, tin/silver, tin/zinc, indium, and indium/silver bi-metallic nanoparticles were synthesized using the wet-chemical methods. The nanoparticles were then characterized with x-ray fluorescence to evaluate the elemental composition and differential scanning to determine the melting point and mass loss of the samples. Results continue to show that bi-metallic nanoparticles are a viable pathway for the fabrication of high-resolution AM melt wires.

Page intentionally left blank

ACKNOWLEDGEMENTS

This work was supported through the Department of Energy Nuclear Energy Enabling Technologies Advanced Sensors and Instrumentation program, under DOE Idaho Operations Office Contract Number DE-AC07-05ID14517. We would like to thank Harry Rollins for his contributions towards melting point characterization with Differential Scanning Calorimetry (DSC).

Page intentionally left blank

CONTENTS

FIGURES

TABLES

ACRONYMS

AM	Advanced Manufacturing
BiPt	Bismuth:Platinum
DEG	Diethylene glycol
DSC	Differential Scanning Calorimetry
DW	Direct Write
InAg	Indium:Silver
NEET ASI	Nuclear Energy Enabling Technologies Advanced Sensors and Instrumentation
PVP	Polyvinylpyrrolidone
RPM	Rotations per minute
SnZn	Tin:Zinc
TXRF	Total Reflection X-Ray Fluorescence
V	Volt

Page intentionally left blank

Multicomponent Nanoparticle Synthesis for Advanced Manufactured Melt Wire Development

1. INTRODUCTION

Advanced manufacturing (AM) has emerged as the predominant enabler for innovation and design for sensors and electronics as it significantly expands the design envelope in terms of materials, form, and functionality. Additionally, these technologies enable rapid prototyping, reduced production cost, and reduced material waste in comparison to classical fabrication methods. As part of the AM focus of the Nuclear Energy Enabling Technologies Advanced Sensors and Instrumentation (NEET ASI) Program, Idaho National Laboratory and Boise State University have recently established in-house capabilities to develop, fabricate, and test new advanced-manufactured sensors, such as those for measuring peak irradiation temperature within a nuclear test reactor. The exploration of novel technologies allows for the development of unique sensors that are not achievable with conventional fabrication processes, and the ability to produce miniature and robust sensors is made possible with additive-manufacturing techniques known as direct-write (DW) technologies, such as aerosol jet printing, plasma-jet printing, inkjet printing, and micro-dispense printing. These technologies are capable of consistently producing device features from 10 to 25 µm, and these size ranges are advantageous for those instances where the miniaturization of sensors is required due to space limitations within an experiment.[1]

A limiting factor for implementing DW technologies in nuclear instrumentation fabrication is the current selection of commercially available feedstock materials that are compatible with these technologies. However, the database of materials available for DW technologies is rapidly expanding and benefitting greatly from emerging nanomaterials development, and efforts are currently being made to significantly expand the library of AM materials to include those that are more relevant to nuclear. These efforts provide the necessary path towards incorporating these novel methods for nuclear energy applications, and such material breakthroughs will revolutionize in-pile sensor development and deployment for the monitoring of nuclear fuel and material behavior during an irradiation experiment.

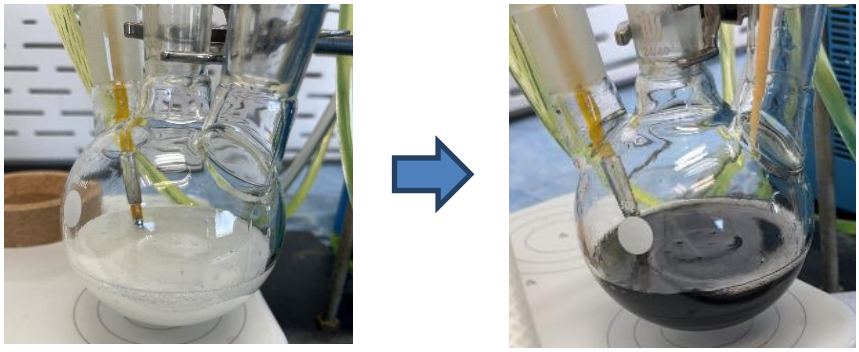

Figure 1. Nanoparticle synthesis: (left) Metallic nanoparticle precursors in solution and (right) nanoparticle formation indicated by color change and formation of black suspension.

Methods for ink synthesis encompass both top-down and bottom-up methods. This process begins with nanoparticles of the metal, ceramic, or alloy of interest in the form of a powder or a dispersion. The key challenges of the top-down approach are found in obtaining a homogenous dispersion of the functional material with a solvent system compatible with DW technologies, limited control over particle size, and large particle size distributions. On the other hand, bottom-up methods for metallic nanoparticles require the synthesis of nanoparticles from their metallic precursors. A schematic for the bottom-up approach is in Figure 1. A capping agent, which induces steric stabilization to minimize agglomeration, is employed to enhance suspension stability and is a critical factor in producing AM feedstock for DW technologies. The bottom-up approach is the preferred method, as it allows for greater control over particle size and size distribution, which are key properties of affecting the quality of the ink formulation. Key challenges associated with bottom-up methods include the development of an appropriate synthesis method, isolation of desired particle shape, particle size and distribution, and identification of an appropriate capping agent.

Irradiation testing is used to gain insight on a wide range of radiation-induced phenomena to understand the performance of fuels and materials in reactor environments. Temperature is a key parameter for irradiation tests, and temperature monitoring is accomplished through both passive and active monitoring techniques. Melt wires are a passive monitoring technique that enable experimenters to identify the peak temperature achieved during an irradiation test.[2,3] This method involves placing wires that have both a known composition and well-characterized melting temperature within a test. The peak test temperature is then inferred during a post-test examination or post-irradiation examination as the wire is inspected for visual signs of melting. Melting shows that the peak temperature during testing exceeded the melting point of wire material. On the other hand, the peak test temperature remained below the melting point of the wire material if the wire does not show signs of melting. Preferably, materials chosen for melt wires have a low neutron-absorption cross section while exhibiting distinct and reproducible melting behavior when they have been exposed to temperatures beyond their respective melting point.

The incorporation of classically fabricated melt wires can be limited due to space and temperature monitoring requirements of irradiation tests, and the motivation for this work is in expanding the temperature monitoring range to provide better temperature spatial resolution than what can be achieved through traditional melt wires. The current list of melt wire materials can be found in Table 1, and large gaps in measurable temperatures are highlighted.[3] To improve the temperature resolution of melt wires, AM methods are being investigated with the development of bi-metallic systems compatible with those AM methods. Current efforts are focused on demonstrating the ability to synthesize a variety of multicomponent metallic nanoparticles from bottom-up methods to enable the fine tuning of temperature resolution by tailoring the melt wire composition, which directly impacts passive peak temperature monitor performance.

Table 1. Current list of materials for classical melt wires.

Material (wt% of components)	Melt Onset (°C)	
56.2Bi33.8Pb10Sn	85.0	
65Bi35In	110.6	
55.2Bi44.8Pb	126.4	
57Bi43Sn	139.4	Δ92.4 °C
100Sn	231.8	
95Sn5Sb	238.6	
90Pb10Sb	252.4	
80Au20Sn	279.5	
90Pb7.5Sn2.5Ag	290.0	
97.5Pb2.5Ag	302.9	
97.5Pb5Ag5Sn	304.0	
97.5Pb1.75Sn1.75Ag	309.3	
100Pb	327.5	
100Zn	479.6	
80Sb20Zn	507.8	Δ152.7°C
100Al	660.5	
49Ag16Cu23Zn7.5Mn4.5Ni	681.3	Δ169.4°C
40Ti20Zr20Cu20Ni	850.7	
98.2Cu1.8Be	865.1	
100Ge	938.3	
82Au18Ni	955.0	
100Ag	961.9	
65Cu35Au	995.6	
100Au	1064.0	
100Cu	1084.6	
70Cu30Ni	1191.0	Δ176.0°C
28Mo69Ni2Pe1Co1Cr	1370.0	
100Ni	1455.0	

This report highlights the most recent work in the development and optimization of wet-chemical synthesis approaches for multicomponent nanoparticle systems intended for advanced-manufactured melt wire development. For this work, single and multicomponent metal nanoparticles were synthesized of bismuth, bismuth/platinum, tin, tin/zinc, tin/silver, indium, and indium/silver. Nanoparticle characterization was accomplished with the use of Differential Scanning Calorimetry (DSC), and Total X-Ray Fluorescence (TXRF) to evaluate their melting point and bulk composition to assess their potential for use as additively manufactured melt wire feedstock materials. These single and multicomponent metal nanoparticles were chosen because they are not commercially available. Due to the limited availability of feedstock materials and inks available for DW technology, a major focus of this project within the NEET ASI program is the development of unique feedstock to enable the fabrication of advanced sensors for in-pile application.

2. MATERIALS AND METHODS

2.1 Materials

Single and multicomponent metal nanoparticles were synthesized using the following materials: diethylene glycol (DEG) (Reagent Plus 99%, Sigma Aldrich), sodium borohydride (99.99 trace metal basis, Sigma Aldrich), bismuth acetate (99.99%, Sigma Aldrich), polyvinylpyrrolidone (Sigma Aldrich), zinc acetate (99.99% trace metals basis, Sigma Aldrich), tin acetate (99.99%, Sigma Aldrich), silver nitrate (99.9999%, Sigma Aldrich), hexachloroplatinate acid (99.9999%, Sigma Aldrich), and indium chloride (99.999% trace metals basis, Sigma Aldrich). Materials used for the XRF included Dow Corning high vacuum grease and a quartz disc for each sample. DSC/TGA was conducted with alumina crucibles (DSC Consumables, 6.5 mm × 4 mm). For the purification process, centrifuge tubes were used to hold the suspension of nanoparticles. The metallic pellet was resuspended in ethyl alcohol (>99.5%, Sigma Aldrich) and acetone (Spectrum) throughout the purification process. All chemicals and reactants were used as received, without further modification.

2.2 Methods

2.2.1 Nanoparticle Synthesis and Purification

Nanoparticle synthesis was accomplished using a method described previously, with modifications.[4] Table 2 – Table 4 provide an overview for the entire bi-metallic nanoparticle series that was synthesized, which includes bismuth/platinum, indium/silver, tin/silver, and tin/zinc. To begin, 100 mL of diethylene glycol (DEG) was degassed within a three-neck round bottom flask. The degassing was done under reflux by bringing the solvent up to 200°C while purging under high-argon flow for a minimum of 2 hours. The DEG was allowed to cool to room temperature before adding polyvinylpyrrolidone (PVP). Alongside, the metal salt precursors were dissolved in 10 mL of DEG. Next, sodium borohydride was dissolved in the vigorously stirring DEG and PVP solution and after ten minutes the metallic precursor solution was added dropwise (1 drop/sec) into the diethylene glycol, PVP, and sodium borohydride solution. After the entirety of the metal salt solution was added, the suspension was allowed to stir overnight.

Purification of nanoparticles to include removal of excess PVP capping agent and reaction by-products was accomplished with centrifugation. The processing parameters were as follows: each suspension of nanoparticles was transferred into a centrifuge test tube and placed into the centrifuge (Thermo Scientific, Legend XT). The samples were run at 9000 RPM for 5 minutes. After each run, the supernatant was discarded, the pellet resuspended with ethanol. This was repeated for a minimum of five times for each sample.

Table 2. Bismuth:Platinum series.

Targeted Composition (at.%)	Bismuth (III) Acetate (g)	Hexachloroplatinic Acid (g)	25 kDa Polyvinylpyrrolidone (g)	Sodium Borohydride (g)	Diethylene Glycol (mL)
1:0	2.97	–	4	0.102	100
19:1	0.881	0.058	4	0.101	100
9:1	0.837	0.117	4	0.100	100

Table 3. Tin:Silver and Tin:Zin series.

Targeted Composition (at.%)	Tin (III) Acetate (g)	Zinc (III) Acetate (g)	Silver (III) Acetate (g)	25 kDa Polyvinylpyrrolidone (g)	Sodium Borohydride (g)	Diethylene Glycol (mL)
Tin: Silver (1:0)	0.592	–	–	0.150	0.500	100
Tin:Silver (96.5:3.5)	0.518	–	0.014	0.151	0.502	100
Tin:Zinc (91:9)	0.562	0.043	–	0.151	0.499	100

Table 4. Indium:Silver series.

Targeted Composition (at.%)	Indium (III) Chloride (g)	Silver (III) Acetate (g)	25 kDa Polyvinylpyrrolidone (g)	Sodium Borohydride (g)	Diethylene Glycol (mL)
Indium:Silver (1:0)	0.561	–	1.04	1.01	100
Indium:Silver (4:1)	0.444	0.0857	1.01	1.01	100
Indium:Silver (7:3)	0.400	0.120	1.00	1.00	100

2.2.2 Total X-Ray Fluorescence (TXRF)

Following purification, the samples were prepared for the TXRF (Bruker S2 Picofox). Using a thin layer of silicon vacuum grease on the quartz discs provided for an adhesive surface to deposit the dried powders. Each sample was run for a 1000-second experiment and no standard was used. In each result, silicon was identified as >50% of the composition. However, this was due to the vacuum grease. After accounting for all the elements that were detected, the target metal compositions were converted to atomic percentages, allowing for the comparison of the predicted composition and the experimental.

It is important to note that composition analysis was performed on the bi-metallic system and not on individual particles. Individual particle composition is critical in determining a target peak temperature for each bi-metallic system. Any deviation can be attributed to experimental error, precursor concentration variations, and different reduction potentials associated with the two different elements.

2.2.3 Differential Scanning Calorimetry (DSC)

Differential scanning calorimetry detects endothermic and exothermic transitions, including the determination of transformation temperatures and the enthalpy of solids and liquids as a function of temperature. For analysis, between 5 and 50 milligrams of sample was loaded into an alumina crucible (DSC Consumables, DSC72001). The crucible was closed and placed in the DSC/TGA (STA 449 F3, Netzsch) to run.

3. RESULTS AND DISCUSSION

3.1 XRF

The TXRF analysis was performed with a Bruker S2 Picofox, and the respective bi-metallic compositions can be found in Table 5. It is important to note that composition analysis was performed on the bi-metallic system and not on individual particles. Individual particle composition is critical in determining a target peak temperature for each bi-metallic system.

Nanoparticle compositions were selected from the phase diagram of each binary phase diagram by evaluating the binary composition that would possess the desired melting point. During the synthesis process, metal salt precursors amounts were determined by establishing a targeted mass for each nanoparticle system, and adjusting precursor amounts to create the desired nanoparticle composition.

With TXRF analysis it was determined that the bulk BiPt system is composed of both bismuth and platinum amounts that are close to targeted concentrations, and similar results were observed for the SnAg system. Meanwhile, the bulk concentrations for the SnZn and InAg systems deviated more significantly from theoretical targets, which could be a result of a significant reduction potential difference between the two nanoparticle components (Table 7). This difference will result in one metal ion species preferentially favored for reduction while the other either does not fully reduce, or may even be preferentially oxidized, which creates an unfavorable environment for alloy formation. Additionally, for the two systems having the most deviation, these can be attributed to experimental error, precursor concentration variations, and different reduction potentials associated with the two different elements.

Table 5. TXRF data.

Nanoparticle System	Theoretical Composition (at.%)	Experimental Composition (at.%)
Tin: Zinc	91:9	98.5:1.53
Tin:Silver	96.5:3.50	98.4:1.60
Tin: Silver	1:0	1:0
Bismuth:Platinum (1:0)	1:0	1:0
Bismuth:Platinum (19:1)	19:1	19:1
Bismuth:Platinum (9:1)	9:1	9:1
Indium:Silver (1:0)	1:0	1:0
Indium:Silver (4:1)	4:1	90.7:9.30
Indium:Silver (7:3)	7:3	38.7:11.3

3.2 DSC

The theoretical and actual melting point were estimated from phase diagrams (Figure 2 – Figure 5) and derived from DSC, respectively, which can be found in Table 6.

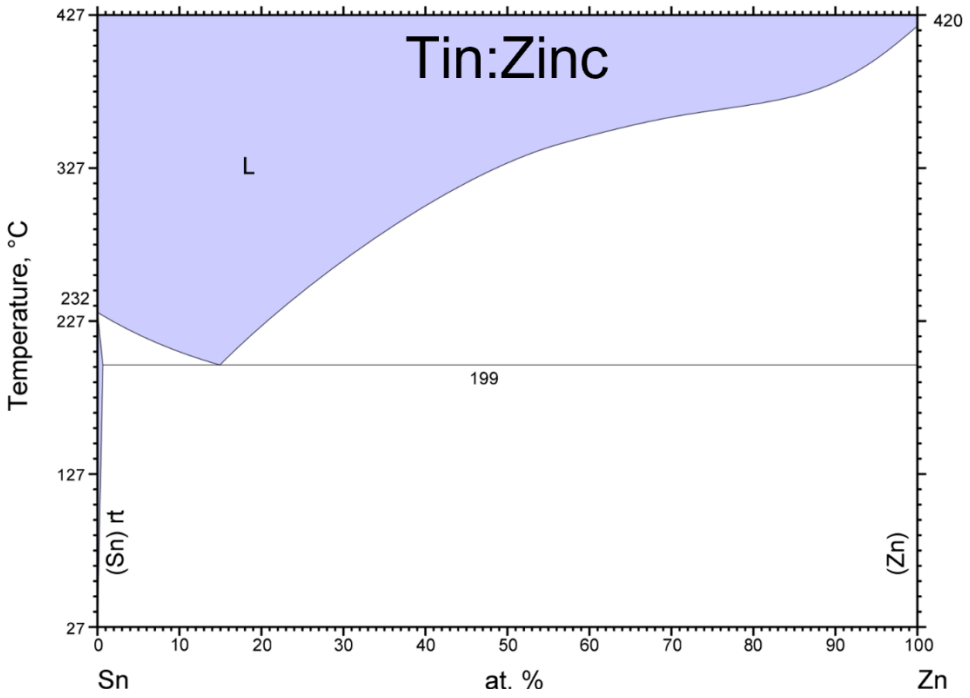

Figure 2. Tin/Zinc phase diagram.[5]

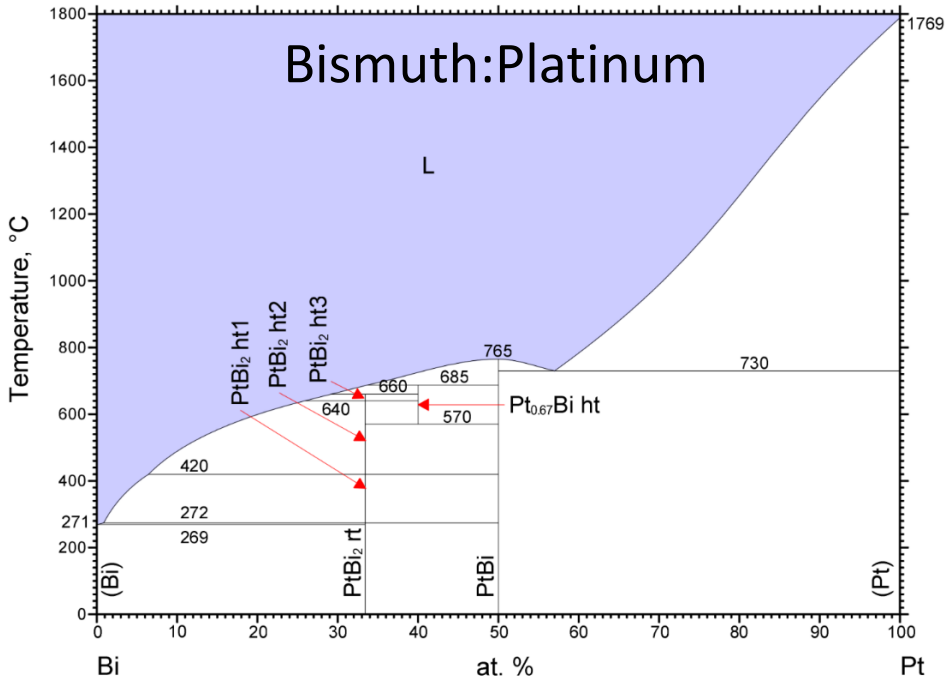

Figure 3. Bismuth/Platinum phase diagram.[6]

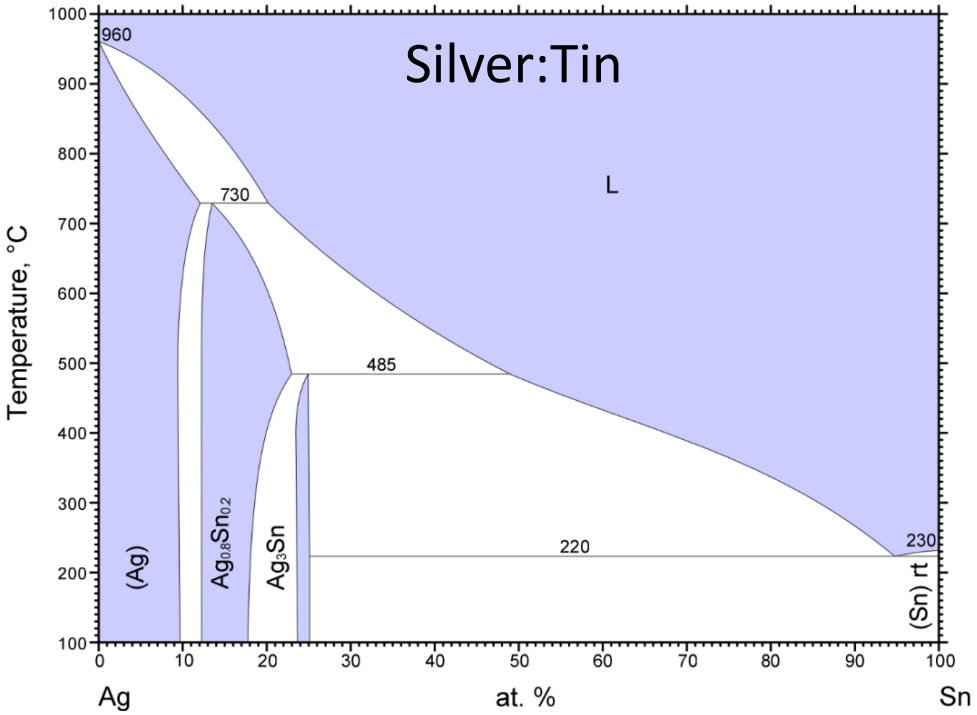

Figure 4. Silver/Tin phase diagram.[7]

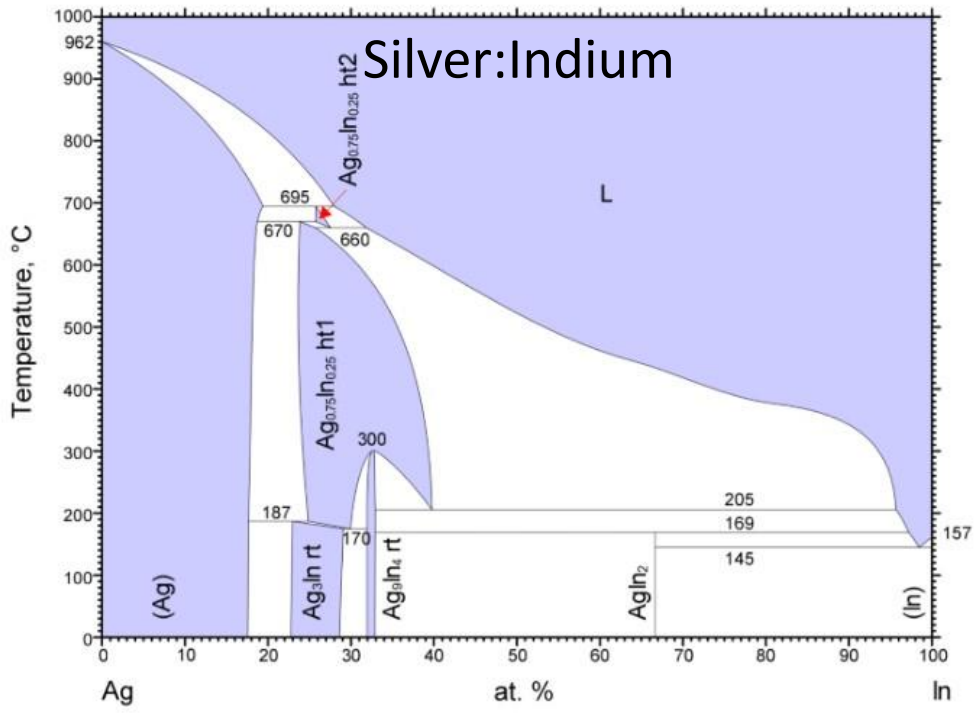

Figure 5. Silver/Indium phase diagram.[8]

Table 6. Melting point of synthesized nanoparticles.

Nanoparticle System	Theoretical Composition (at.%)	Targeted Melting Point (°C)	Theoretical Melting Point* (°C)	DSC Melting Point (°C)
Tin: Zinc	91:9	198	227	231.8
Tin:Silver	96.5:3.50	221	230	219.4
Tin: Silver	1:0	231	231	230.3
Bismuth:Platinum (1:0)	1:0	271	271	271.0
Bismuth:Platinum (19:1)	19:1	400	400	341.9
Bismuth:Platinum (9:1)	9:1	500	500	363.0
Indium:Silver (1:0)	1:0	157	157	157.3
Indium:Silver (4:1)	4:1	340	339	–
Indium:Silver (7:3)	7:3	385	385	–

*Theoretical melting point derived from measured compositions from TXRF

Table 7. Standard Reduction Potential of Nanoparticle Components.[9]

Element	Reduction Half Reaction	E° (V)
Tin (Sn^{2+})	$Sn^{2+} + 2e^- \rightleftharpoons Sn$	-0.14
Zinc (Zn^{2+})	$Zn^{2+} + 2e^- \rightleftharpoons Sn$	-0.76
Silver (Ag^+)	$Ag^+ + e^- \rightleftharpoons Ag$	0.80
Bismuth (Bi^{3+})	$Bi^{3+} + 3e^- \rightleftharpoons Bi$	0.32
Platinum (Pt^{2+})	$PtCl_6^{2-} + 2e^- \rightleftharpoons PtCl_4^{2-} + 2Cl^-$	0.68
	$PtCl_4^{2-} + 2e^- \rightleftharpoons Pt(s) + 4Cl^-$	0.73
Indium (In^{3+})	$In^{3+} + 3e^- \rightleftharpoons In$	-0.34

Continuing work from previous years, the bismuth:platinum system was further investigated, but new ratios for the two components were chosen.[4] To differentiate from previous years, a smaller range of compositions of the two components were selected to provide further understanding for the level of control over both nanoparticle composition and melting point afforded from the chemical reduction process in nanoparticle synthesis. From DSC results for the bismuth:platinum system, it is clear that further optimization of the synthesis process is required along with additional characterization to elucidate the composition of the individual nanoparticles. It is expected that the nanoparticle ratios of bismuth and platinum vary significantly from what was obtained from TXRF based on the significant deviation of the experimental melting point from the theoretical melting point. The reason for this deviation is unknown, but the melting point deviation from theoretical values indicates that the targeted concentration for the individual particles was not achieved such as imperfect alloying resulting in particles having a higher concentration of bismuth or particles having a higher concentration of platinum. To better understand the cause for this, further investigation is required. Looking at it from a different perspective, the melting point of the two different bismuth:platinum nanoparticle compositions provided a melting point range of

21.1°C, which is much smaller than what was achieved previously, and very promising with respect to the goal of increasing the temperature resolution of melt wires.

The second nanoparticle system group was chosen to further support advanced-manufactured melt wire development. For this series of nanoparticles, the current list of melt wire materials was used as a guide for the individual component selection. Then, a review of a range of binary phase diagrams were evaluated to determine which systems would provide a melting point range of less than 100°C if an array consisting of three different advanced-manufactured melt wires were fabricated. From the review, tin:zinc (91:9), tin (100), and tin:silver (96.5:3.50) were selected as meeting those requirements. From previous experiments, if a relatively deep eutectic is observed, the concentration of the nanoparticles will favor that point. So, eutectic compositions were selected for the tin:zinc and tin:silver along with single element tin. The experimental and theoretical melting points for tin:silver and tin were in agreement. However, for tin:zinc the observed melting point was what was expected for tin. Based on the reduction potential difference between the materials and the TXRF results, it is anticipated that the reducing agent used was not appropriate for tin:zinc alloy formation and was unable to effectively reduce zinc during synthesis. As with the bismuth:platinum system, this series demonstrated the ability to vary the melting point of nanoparticles by adjusting particle composition. Additionally, with the tin:silver system, it showed the ability to readily form the composition where a eutectic point exists for materials having similar reduction potentials and using sodium borohydride as the reducing agent.

Finally, with the understanding that a eutectic point existing in a binary system will affect the ability to control nanoparticle composition, the next selection criteria included an evaluation of a binary system having no eutectic, and indium:silver was selected. However, with DSC analysis, no onset of melting was detected except for the pure indium system. It is anticipated that, similar to the tin:zinc system, the significant difference between the reduction potential of indium and silver did not favor alloy formation with the current synthesis method used. It is expected that a stronger reducing agent, such as lithium borohydride, could facilitate the formation of the desired nanoparticle compositions, or additional nanoparticle synthesis routes may need to be investigated, such as laser ablation or ball milling.

The DSC graph for each material can be found in Appendix A.

3.3 Summary

A variety of single and bi-metallic nanoparticles have been synthesized using wet-chemical approaches using a strong reducing agent. This goal of this work was to enhance the temperature resolution of melt wires for peak temperature detection within irradiation tests. With the use of DSC, preliminary results demonstrate further promise towards tailoring the targeted peak temperature of melt wires with the development of bi-metallic nanoparticle systems. The bismuth:platinum, and tin:silver series exhibited varying melting points that correlate to varying compositions that are a direct result of varying the ratio of the metal precursors during synthesis. However, for the bismuth:platinum system achieving the targeted melting point was more elusive and validated the need to further optimize the synthesis process for multicomponent nanoparticles.

This work showed that when using the chemical reduction process for multicomponent nanoparticle synthesis, the consideration of the standard reduction potential for each of the components is critical, and that those values need to be relatively close. Otherwise, reduction of the two materials is not favored, and multicomponent nanoparticle formation will not occur.

Next steps will include further optimization of the synthesis process to minimize error associated with synthesizing bi-metallic nanoparticles of specific composition, and the exploration of additional synthesis methods to facilitate the formation of nanoparticle alloys with certain material combinations that are not necessarily favored with the use of wet-chemical reduction process based on sodium borohydride. From the melting points obtained via DSC for the different multicomponent systems having single components with relatively close reduction potentials, the melt wires printed from these materials are expected to have better temperature resolution than those classically manufactured melt wires fabricated from bulk metals.

4. REFERENCES

1. Seifert, T., E. Sowade, F. Roscher, M. Wiemer, T. Gessner, and R. R. Baumann. "Additive Manufacturing Technologies Compared: Morphology of Deposits of Silver Ink Using Inkjet and Aerosol Jet Printing." *Industrial & Engineering Chemistry Research* 54, no. 2 (2015): 769–779. https://doi.org/10.1021/ie503636c.
2. Daw, J. E., J. L. Rempe, D. L. Knudson, T. C. Unruh, B. M. Chase, K. L. Davis, and A. J. Palmer. "Temperature monitoring options available at the Idaho national laboratory advanced test reactor." *AIP Conference Procedure* 1552, (2013): 970. https://doi.org/10.1063/1.4819675.
3. Davis, K. L., D. L. Knudson, J. E. Daw, J. L. Rempe, and A. J. Palmer. "Melt wire sensors available to determine peak temperatures in ATR irradiation testing." *8th International Topical Meeting on Nuclear Plant Instrumentation, Control, and Human-Machine Interface Technology 2012: Enabling Future Nuclear Energy* 1, (2012): 427–434. ISBN: 978-1-62748-015-4.
4. Fujimoto, K. T., and M. D. McMurtrey. (2021). *Development of Bismuth and Platinum Bi-Metallic Nanoparticles to Enhance Melt Wire Temperature Resolution*. INL/EXT-21-63525-Rev000. Idaho National Laboratory, Idaho Falls, ID (United States).
5. Moser Z., J. Dutkiewicz, W. Gasior, and J. Salawa. *Sn-Zn Phase Diagram, ASM Alloy Phase Diagrams Database*. P. Villars, editor-in-chief; H. Okamoto and K. Cenzual, section editors; http://www.asminternational.org. ASM International, Materials Park, OH, 1990.
6. Okamoto, H., *Bi-Pt Phase Diagram, ASM Alloy Phase Diagrams Database*. P. Villars, editor-in-chief; H. Okamoto and K. Cenzual, section editors; http://www.asminternational.org. ASM International, Materials Park, OH, 1991.
7. Gierlotka W., Y. C. Huang, and S. W. Chen. *Ag-Sn Phase Diagram, ASM Alloy Phase Diagrams Database*. P. Villars, editor-in-chief; H. Okamoto and K. Cenzual, section editors; http://www.asminternational.org, ASM International, Materials Park, OH, 2008.
8. Baren M. R. *Ag-In Phase Diagram, ASM Alloy Phase Diagrams Database*, P. Villars, editor-in-chief; H. Okamoto and K. Cenzual, section editors; http://www.asminternational.org. ASM International, Materials Park, OH, 2016.
9. S. G. Bratsch, "Standard Electrode Potentials and Temperature Coefficients in Water at 298.15 K." *J. Phys. Chem.* 18, no. 1. (1989).

Appendix A

DSC Graphs

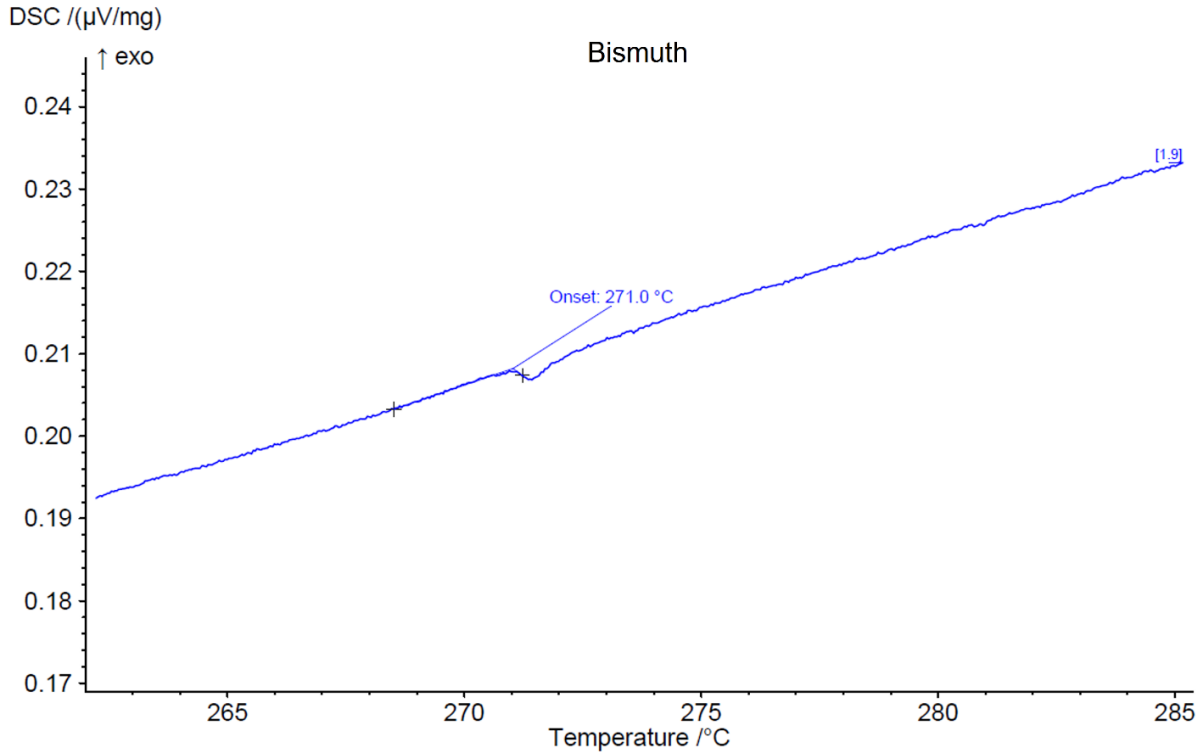

Figure A1. Bismuth DSC graph having an onset at 271.0°C.

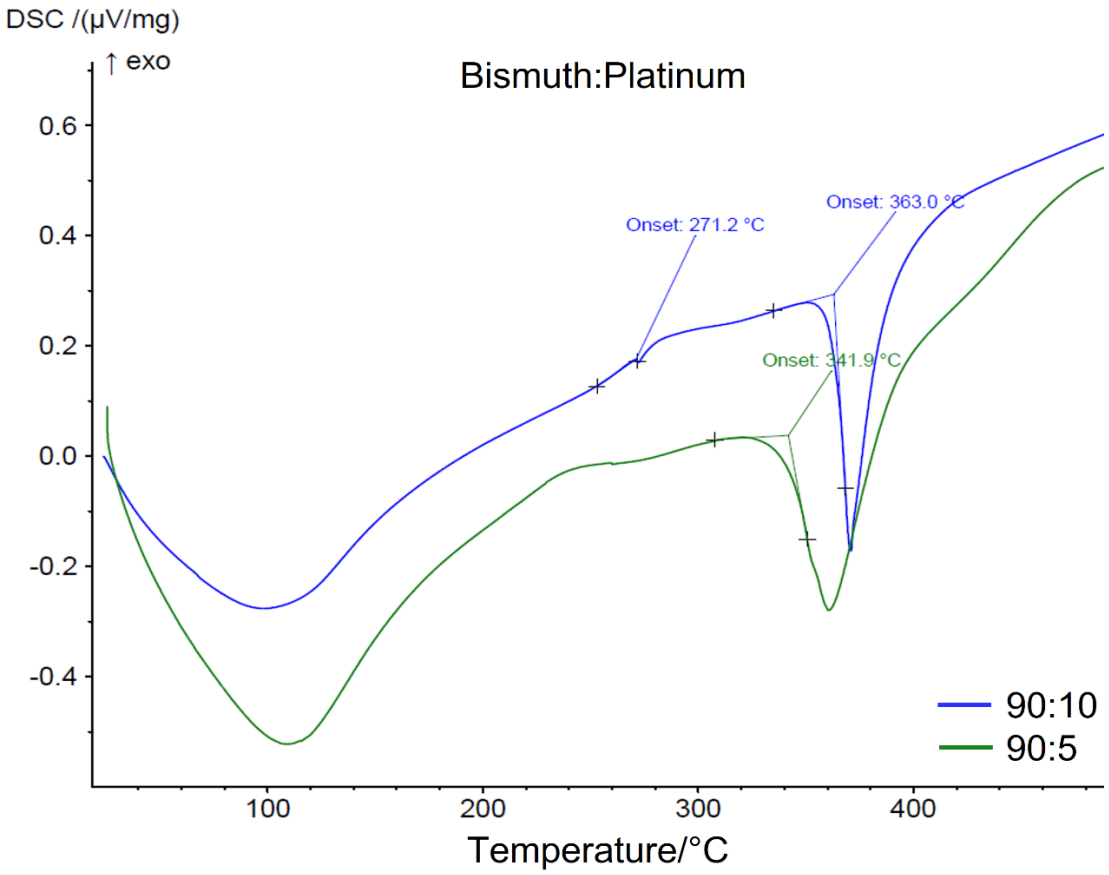

Figure A2. Bismuth:Platinum DSC graph for 90:10 exhibiting a melt onset at 271.2°C and 363.0°C and 90:5°C exhibiting a melt onset of 341.9°C.

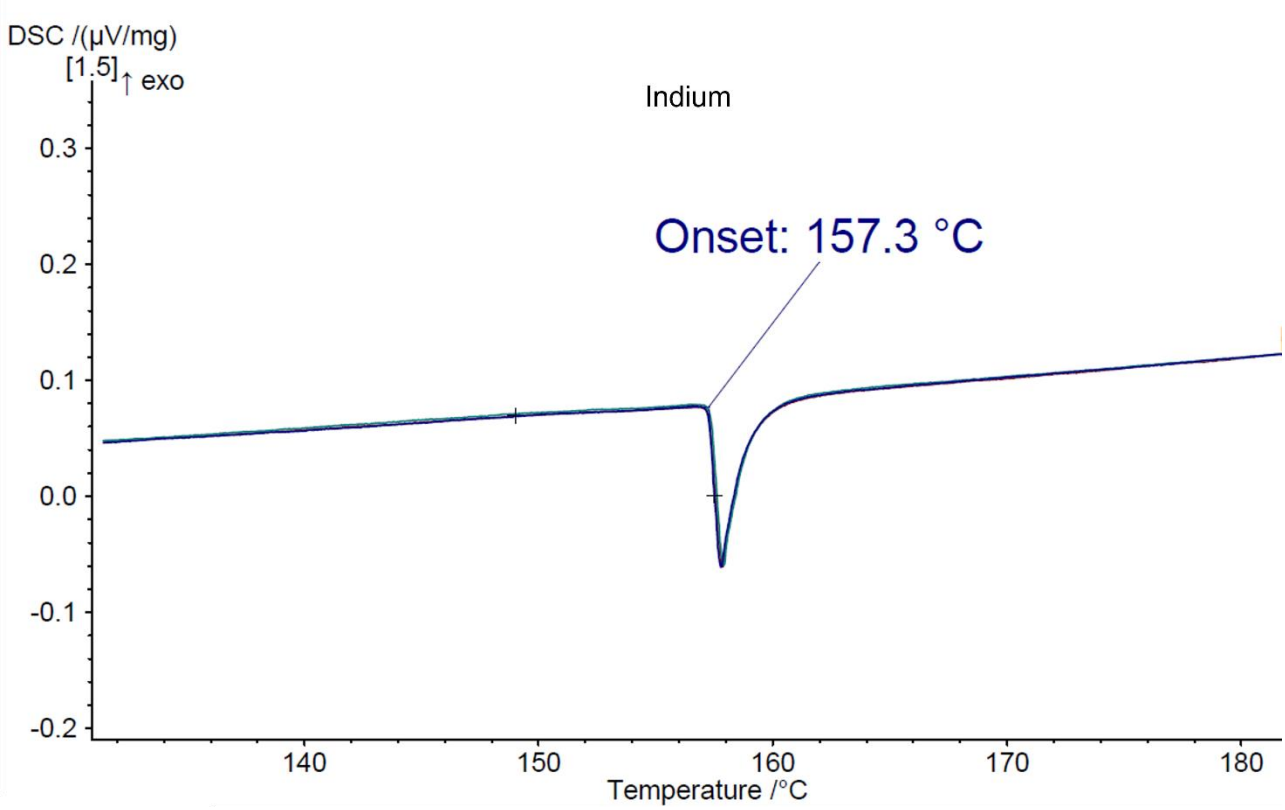

Figure A3. Indium DSC graph exhibiting a melt onset at 157.3°C.

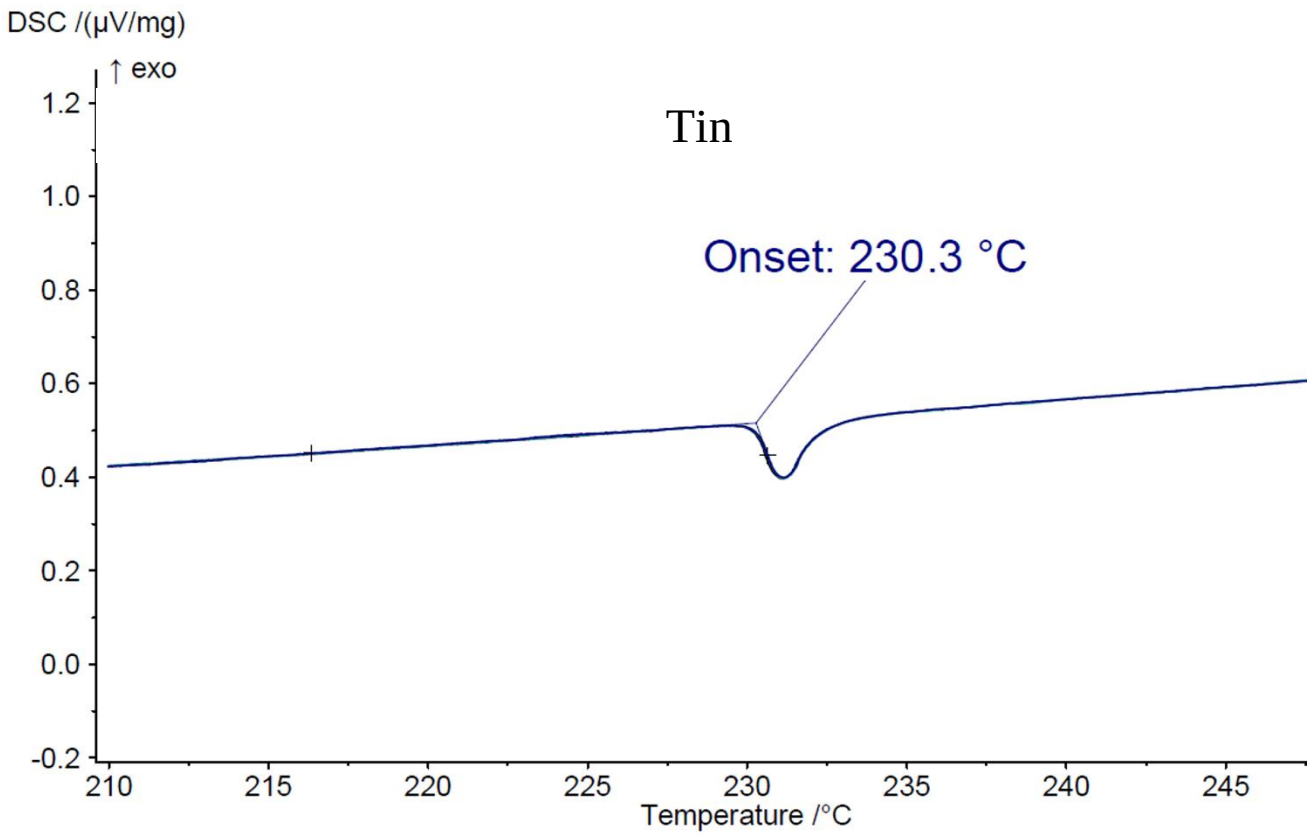

Figure A4. Tin DSC graph exhibiting a melt onset at 230.3°C.

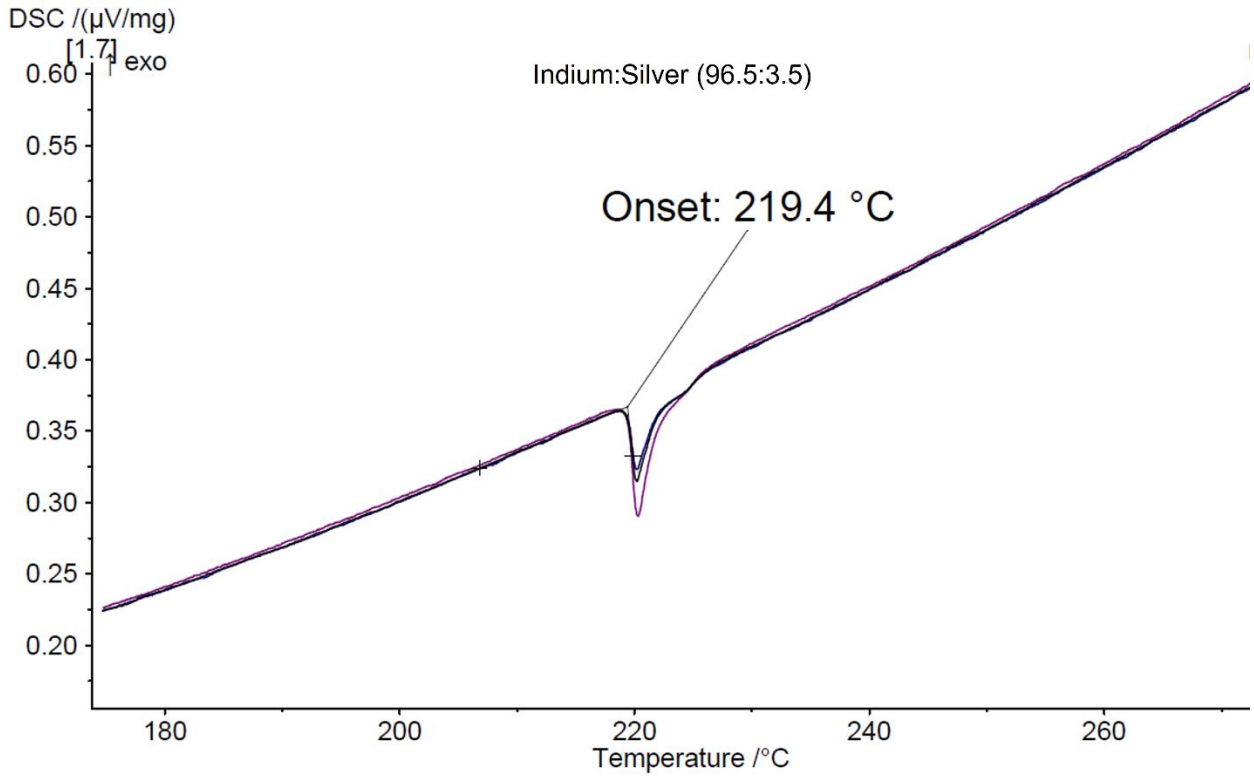

Figure A5. Indium:Silver (96.5:3.5) DSC graph exhibiting a melt onset at 219.4°C.

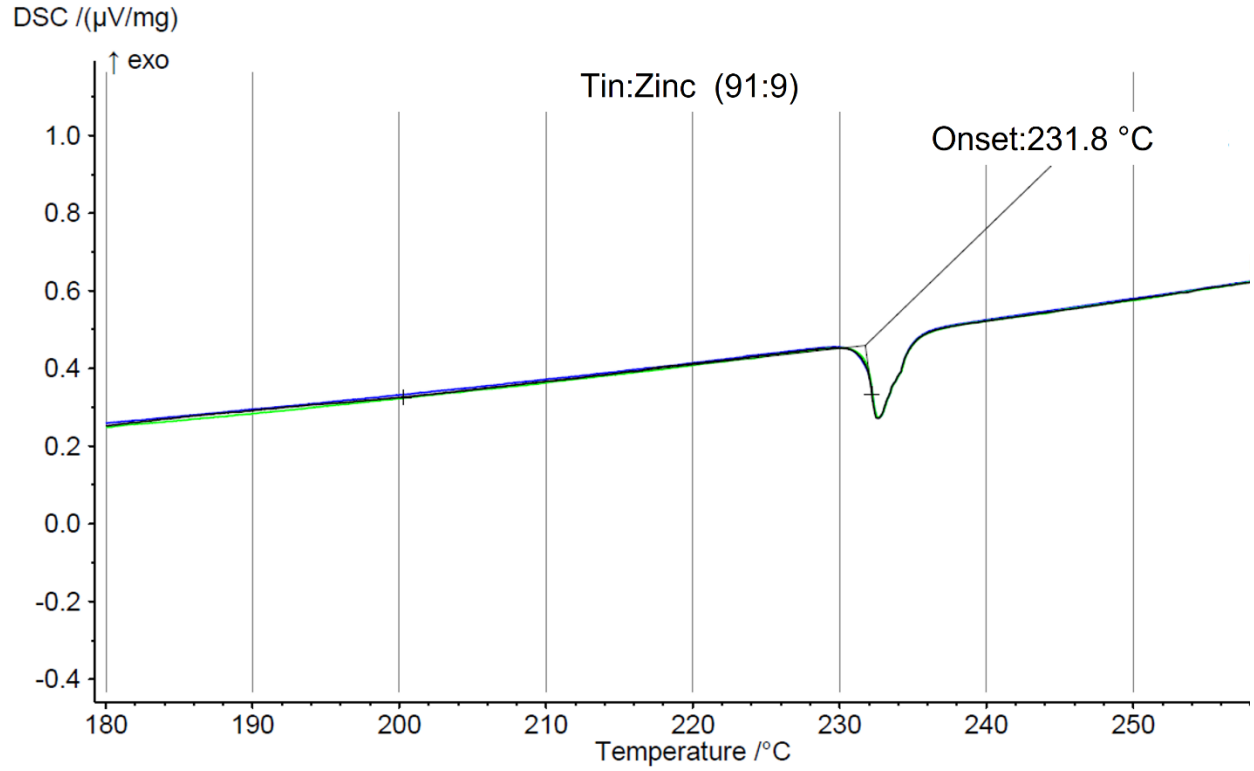

Figure A6. Indium:Zinc (91:9) DSC graph exhibiting a melt onset at 231.8°C.